Hindawi
Complexity
Volume 2020, Article ID 6786832, 11 pages
https://doi.org/10.1155/2020/6786832

Research Article

Analysis, Stabilization, and DSP-Based Implementation of a Chaotic System with Nonhyperbolic Equilibrium

Xuan-Bing Yang,[1,2] Yi-Gang He ,[1,3] Chun-Lai Li ,[2] and Chang-Qing Liu[1]

[1]*School of Electrical Engineering and Automation, Hefei University of Technology, Hefei 230009, China*
[2]*School of Information Science and Engineering, Hunan Institute of Science and Technology, Yueyang 414006, China*
[3]*School of Electrical Engineering and Automation, Wuhan University, Wuhan 430072, China*

Correspondence should be addressed to Yi-Gang He; 18655136887@163.com and Chun-Lai Li; hnistlichl@163.com

Received 31 August 2019; Revised 21 October 2019; Accepted 13 November 2019; Published 8 January 2020

Guest Editor: Viet-Thanh Pham

This paper reports an autonomous dynamical system, and it finds that one nonhyperbolic zero equilibrium and two hyperbolic nonzero equilibria coexist in this system. Thus, it is difficult to demonstrate the existence of chaos by Šil'nikov theorem. Consequently, the topological horseshoe theory is adopted to rigorously prove the chaotic behaviors of the system in the phase space of Poincaré map. Then, a single control scheme is designed to stabilize the dynamical system to its zero-equilibrium point. Besides, to verify the theoretical analyses physically, the attractor and stabilization scheme are further realized via DSP-based technique.

1. Introduction

Chaotic behaviors exist widely in biology, engineering, economy, and many other scientific disciplines [1–4]. Chaotic systems have the properties of unpredictability, topological mixing, ergodicity, and sensitivity to their initial values and control parameters. Owing to the noise-like spectrum and broad-band, chaotic signals are potentially applicable in engineering such as random sequence generation [5], secure communication [6], image encryption [7, 8], signal detection [9], radar and sonar systems [10], and so on. Therefore, it is significant to design and analyze new chaotic systems. In 1963, Lorenz proposed the first three-dimensional chaotic system when studying earth's atmospheric convection [11]. Then, many low-dimensional mathematical models with positive Lyapunov exponents have been introduced, along with the analysis of a rich class of dynamical behaviors. New examples continue to be reported for publication in nonlinear dynamics journals for the physical applications. Nevertheless, it is necessary to develop chaotic systems with simple structure and rich dynamical behaviors from the perspective of application.

As a striking chaos theory with symbolic dynamics obtained by Kennedy in continuous map [12], the topological horseshoe can provide an impactful tool for proving chaotic dynamics in hyperbolic or nonhyperbolic system. Up to present, many noteworthy theoretical progresses have been extended in finding the existence of horseshoe. For example, Yang introduced the remarkable criteria for finding the topological horseshoe in noncontinuous map [13, 14], which has been successfully applied to some practical systems for verifying chaos [15, 16]. Li presented a new method with three steps for finding horseshoes in dynamical systems by using several simple results on topological horseshoes [17]. However, it is still a tough work to find a topological horseshoe in a practical chaotic system [18].

It is impossible to chronically predict the future behavior of chaotic system, but one can stabilize the future behavior into a certain range by using control technology. The seminal attempt of controlling chaos is the well-known OGY method, which applies small perturbations to system parameter to keep the system close to the target periodic orbit [19]. However, the experimental implementation of this

method is restricted by the level of noise in the experimental data for the sake of the discrete nature of the control signal. Then, a continuous delayed feedback scheme is proposed consequently [20]. The control signal is the perturbations of the difference between the states of the current system and one period of the target orbit in the past. Therefore, the intensity of the perturbations will vanish when the system evolves to the desired orbit. Since then, a wide variety of control approaches emerged for different applications, such as backstepping control [21], sliding mode control [22], sampled-data control [23], and multiswitching combination control [24], just to name a few. However, the present schemes focused on the control problem need several controllers. From the points of both practical application and theoretical research, it is significant to design simple yet executable control technique.

In this paper, an autonomous chaotic system with a simple algebraic structure of six terms is proposed. Basic dynamical properties of the system, including equilibrium point, phase portrait, Poincaré map, parameter bifurcation, and Lyapunov exponent, are studied in theory and numerical simulation. It is found that this system exhibits fruitful dynamic behaviors of dense periodic windows and coexistence of nonhyperbolic and hyperbolic equilibrium points. And to rigorously verify the emergence of chaos of this system in theory, the topological horseshoe is investigated in the phase space of Poincaré map. Then, based on the Lyapunov stability criterion, a single control scheme is designed to stabilize the chaotic system to its zero-equilibrium point. The implementation scheme of attractors and control scheme are discussed in detail and realized via DSP-based technique, confirming the validity and enforceability of the theoretical scheme.

2. The Proposed Dynamical System

The autonomous dynamical system considered here is given by

$$\begin{cases} \dot{x}_1 = -ax_1 + bx_2, \\ \dot{x}_2 = ex_2 - fx_1x_3, \\ \dot{x}_3 = -cx_3^3 + dx_1x_2. \end{cases} \tag{1}$$

Differential equations of system (1) are simple with a cubic term and two quadratic cross-product terms. The system parameters a, b, c, d, e, and f are all positive constants.

2.1. Dissipativity and Existence of Attractor. We first consider the general condition of dissipativity to ensure the chaotic property:

$$\nabla V = \frac{\partial \dot{x}_1}{x_1} + \frac{\partial \dot{x}_2}{x_2} + \frac{\partial \dot{x}_3}{x_3} = -a + e - 3cx_3^2. \tag{2}$$

Therefore, system (1) would be dissipative and will converge to a subset of measure zero volume according to $dV/dt = e^{(-a+e-3cx_3^2)}$, when satisfying $-a + e - 3cx_3^2 < 0$. This means that the volume will become $V(0)e^{(-a+e-3cx_3^2)t}$ at time t through the flow generated by the system for an initial volume $V(0)$. Therefore, there exists an attractor in system (1) with $-a + e - 3cx_3^2 < 0$.

2.2. Equilibrium Points and Stability. Considering the condition of equilibrium point $\dot{x}_1 = 0$, $\dot{x}_2 = 0$, and $\dot{x}_3 = 0$, we obtain three equilibrium points of system (1), as follows:

$$\begin{aligned} &P_0(0, 0, 0), \\ &P_1\left(\frac{a}{b}\sqrt{\frac{ce^3}{df^3}}, \frac{a^2}{b^2}\sqrt{\frac{ce^3}{df^3}}, \frac{ae}{bf}\right), \\ &P_2\left(-\frac{a}{b}\sqrt{\frac{ce^3}{df^3}}, -\frac{a^2}{b^2}\sqrt{\frac{ce^3}{df^3}}, \frac{ae}{bf}\right). \end{aligned} \tag{3}$$

When selecting $a = 1$, $b = 6$, $c = 5$, $d = 1$, $e = 3$, and $f = 2$, the equilibrium points and the corresponding eigenvalues are shown in Table 1, including the type of equilibrium points.

From Table 1, it is known that the three equilibrium points are all unstable with stable manifold and unstable manifold. According to [25], since the characteristic value λ_3 of equilibrium point P_0 equals to zero, the equilibrium point is nonhyperbolic type. However, equilibrium points P_1 and P_2 are hyperbolic since all the real parts of the corresponding eigenvalues of these two equilibrium points are nonzero. Therefore, this is a chaotic system in which hyperbolic and nonhyperbolic equilibrium points coexist. And, this kind of chaotic system does not belong to Šil'nikov sense of the chaotic system, and it is difficult to prove the existence of chaos by Šil'nikov theorem. At present, chaotic systems with special features, such as chaotic systems with nonequilibrium, with multistability and with hyperbolic and nonhyperbolic equilibrium coexisting, have attracted extensive attention by researchers [26, 27].

2.3. Phase Portrait and Chaotic Properties. When selecting $a = 1$, $b = 6$, $c = 5$, $d = 1$, $e = 3$, $f = 2$, and initial values $x(0) = (0.01, 0.01, 0.05)$, the Lyapunov exponents of system (1) are depicted in Figures 1(a) and 1(b) with the values as 0.123017, 0.000029, and −11.414797. According to the three Lyapunov exponents, the Kaplan–Yorke dimension is $D_{KY} = 2 + (0.123017 + 0.000029)/11.414797 = 2.0108$. Therefore, the Kaplan–Yorke dimension is fractional. The corresponding chaotic phase diagrams further reveal that the proposed system displays complicated chaotic behaviors, as depicted in Figure 2.

As an important analytical technique, Poincaré map can reflect the bifurcation and folding properties of chaos. Selecting the parameter values $a = 1$, $b = 6$, $c = 5$, $d = 1$, $e = 3$, and $f = 2$ and taking the crossing planes $x_3 = 0$, $x_1 = 0$, and $x_2 = 0$, we obtain the corresponding Poincaré maps illustrated in Figure 3. We can see the attractor structure from the dense dots.

2.4. Influence of Parameter Variation. It is found that system (1) exhibits complicated dynamical behaviors with the

Table 1: Equilibrium points and eigenvalues of system (1).

Equilibrium point	Eigenvalues	Type of equilibrium point
P_0 (0, 0, 0)	$\lambda_1 = -1$, $\lambda_2 = 3$, $\lambda_3 = 0$	Nonhyperbolic
P_1 (0.6847, 0.1141, 0.25)	$\lambda_1 = 1.1087 + 0.6279i$, $\lambda_2 = 1.1087 - 0.6279i$, $\lambda_3 = -1.1549$	Hyperbolic
P_2 (–0.6847, -0.1141, 0.25)	$\lambda 1 = 1.1087 + 0.6279i$, $\lambda 2 = 1.1087 - 0.6279i$, $\lambda 3 = -1.1549$	Hyperbolic

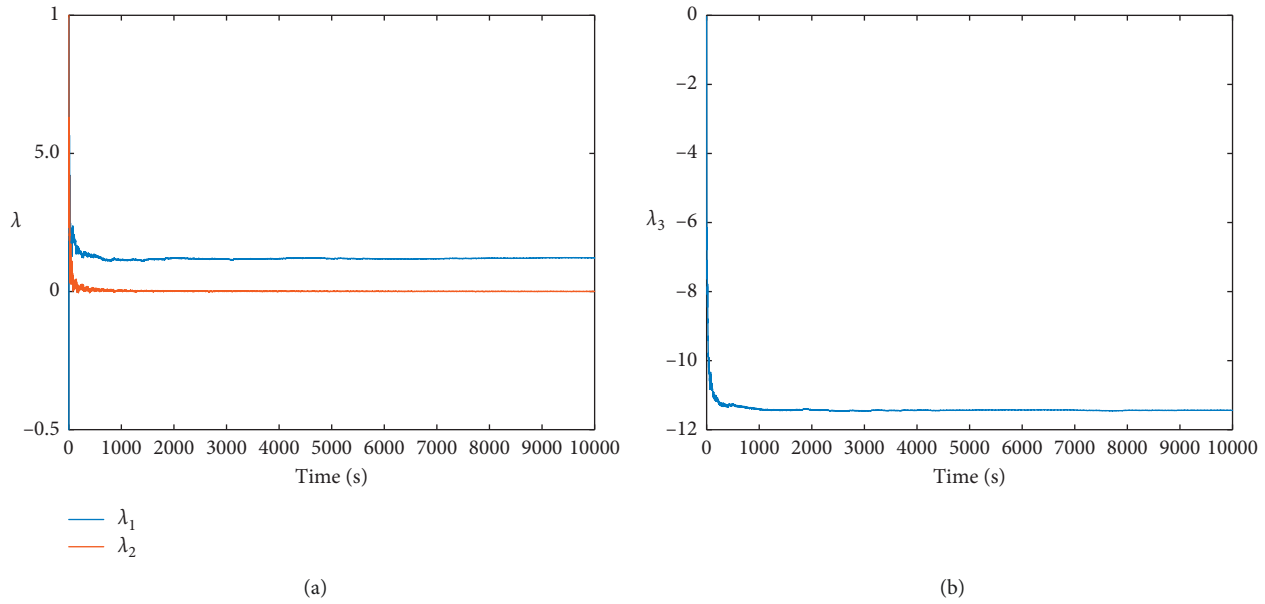

Figure 1: Lyapunov exponents of system (1) when $a = 1$, $b = 6$, $c = 5$, $d = 1$, $e = 3$, and $f = 2$.

variation of system parameters. As explication, we only consider the variation of parameters c and f in this section.

When fixing parameters $\{a = 1, b = 6, d = 1, e = 3, f = 2\}$ and letting c vary from 2 to 8, the corresponding bifurcation diagram of state variable x_3 and the maximum Lyapunov exponent of system (1) versus c of numerical calculation are shown in Figures 4(a) and 4(b), respectively. As we know that system (1) shows rich dynamical behaviors, ranging from stable equilibrium points, periodic orbits to chaotic oscillations, depending on the parameter values. Furthermore, there emerge many visible periodic windows in the chaotic region. Then, we fix parameters $a = 1$, $b = 6$, $c = 5$, $d = 1$, and $e = 3$, while letting f vary from 1 to 3. Figures 5(a) and 5(b) depict the bifurcation diagram of state variable x_3 and the maximum Lyapunov exponent of system (1) versus parameter f, respectively. It is known that with the variation of parameter f, system (1) ranges from stable equilibrium points, periodic orbits to chaotic oscillations, and there emerges many densely distributed periodic windows in the chaotic region, also showing the rich dynamics. The variation of the properties of system (1) with system parameters c and f is of great importance in image encryption.

3. Topological Horseshoe in the Dynamical System

3.1. Review of Topological Horseshoe Theorems. It is still a challenge to find topological horseshoes in a concrete system, especially to select a suitable quadrilateral in the cross section. Before studying the horseshoe embedded in the dynamical system, some theorems on topological horseshoe are reviewed below [12–14, 17].

Let D be a compact subset of S, which is a metric space, and there exists m mutually disjoint compact subsets $D_1, D_2, \ldots, D_m$ of D.

Definition 1. Let $D_i^1, D_i^2 \subset D_i$ be two fixed disjoint compact subsets with $1 \le i \le m$. If $\gamma \cap D_i^1$ and $\gamma \cap D_i^2$ are compact and nonempty, we say that the connected subset γ of D_i connects D_i^1 and D_i^2, and denote this by $D_i^1 \overset{\gamma}{\leftrightarrow} D_i^2$.

Definition 2. Let γ be a connected subset of D_i, we say that $f(\gamma)$ is suitably across D_i with respect to D_i^1 and D_i^2, if there is a connected subset $\gamma_i \subset \gamma$ satisfying $f(\gamma_i) \subset D_i$, and $f(\gamma_i) \cap D_i^1$ and $f(\gamma_i) \cap D_i^2$ are nonempty. In this case, it is denoted by $f(\gamma) \longmapsto D_i$.

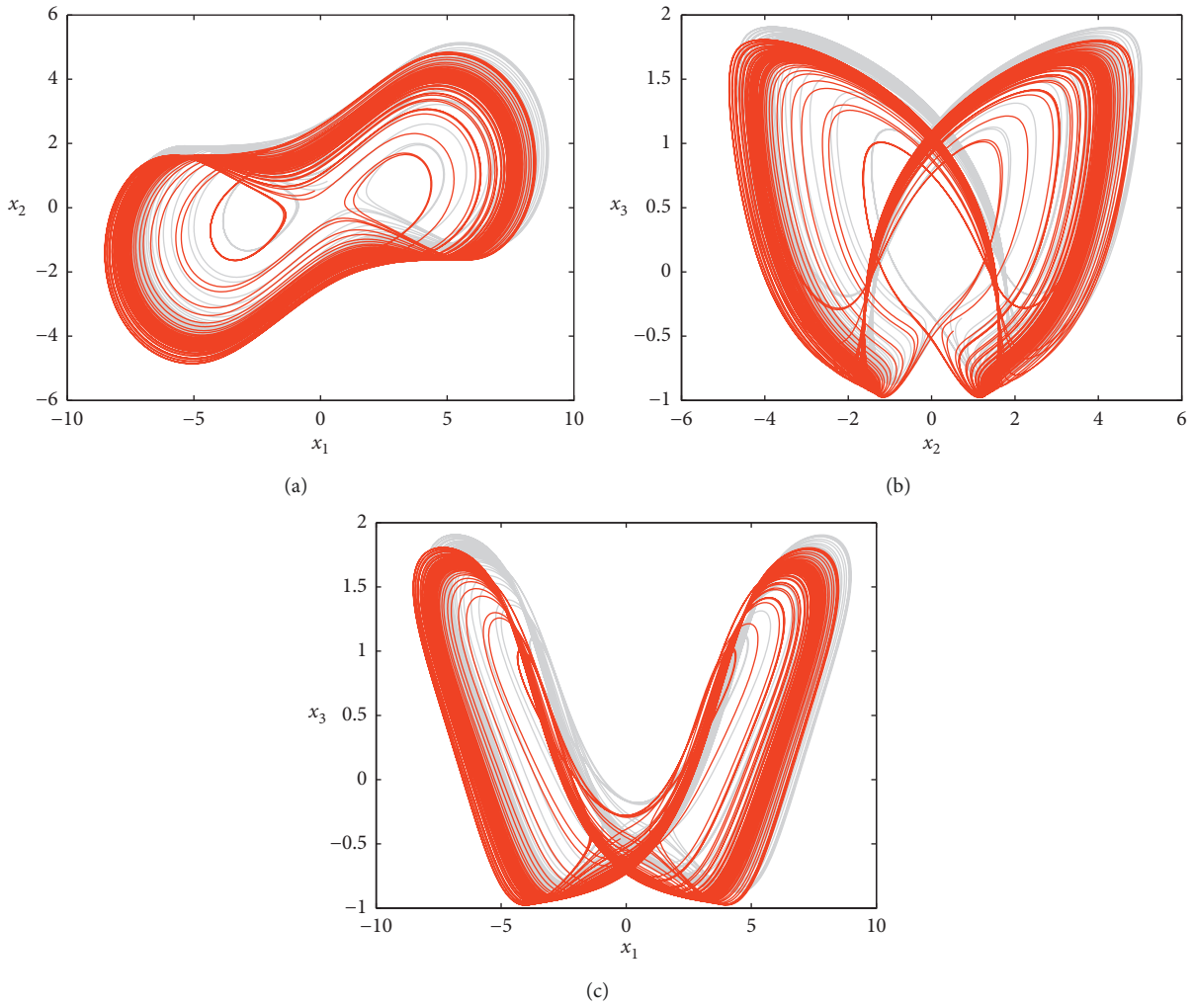

Figure 2: Chaotic phase diagrams of the proposed system.

Definition 3. Suppose that σ: $\Sigma m \longrightarrow \Sigma m$ and f: $S \longrightarrow S$ are both continuous functions with topological spaces Σm and S, respectively. If there exists a continuous surjection h: $\Sigma m \longrightarrow S$ confirming to $f \circ h = h \circ \sigma$, it is said that f is topologically semiconjugate to function σ.

Lemma 1. *If $f^p(D_i) \longmapsto D_i$, then we have $f^{mp}(D_i) \longmapsto D_i$, where m is a positive integer.*

Lemma 2. *If $f^p(D_1) \longmapsto D_1$, $f^p(D_1) \longmapsto D_2$, $f^q(D_2) \longmapsto D_1$, and $f^q(D_2) \longmapsto D_2$, then there would exist a compact invariant set $M \subset D$, such that $f^{p+q} \mid M$ is semiconjugate to 2-shift dynamics and the topological entropy of f will satisfy $ent(f) \geq [1/(p+q)]\log 2$.*

3.2. Finding Topological Horseshoe in the Dynamical System. According to the theory above, a horseshoe will be found in the dynamical system by three steps [17]. In this process, we set the parameters of system (1) as $a = 1$, $b = 6$, $c = 5$, $d = 1$, $e = 3$, $f = 2$, and initial condition $x(0) = (0.01, 0.01, 0.05)$.

Step 1. As shown in Figure 6, we first select four vertices of the Poincaré section P on the plane $\Theta = \{(x_1, x_2, x_3) \in R^3 : x_2 = 0\}$ as (–8, 0, –0.5), (–8, 0, 1.5), (8, 0, 1.5), and (8, 0, –0.5).

Step 2. Then, after many trial-and-error numerical simulations, we carefully pick a quadrilateral D_1 of quadrangle P, with the four vertices being

$$\begin{aligned} &(-7.618610595, 0, 1.062250623) \\ &(-7.643703532, 0, 1.049345387) \\ &(-7.239428439, 0, 1.018765586) \\ &(-7.215729554, 0, 1.031951372). \end{aligned} \tag{4}$$

Let us suppose that D_1^1 denotes the left side while D_1^2 denotes the right side of quadrilateral D_1. It is known from the numerical result that the third return map $H^3(D_1^1)$ lies on the left side of D_1, but the third return map $H^3(D_1^2)$ lies on the right side of D_1. Thereby, under this return map, the image $H^3(x)$ $(x \in D_1)$ lies wholly across the quadrangle D_1 with respect to the sides D_1^1 and D_1^2, seen in Figure 7(a).

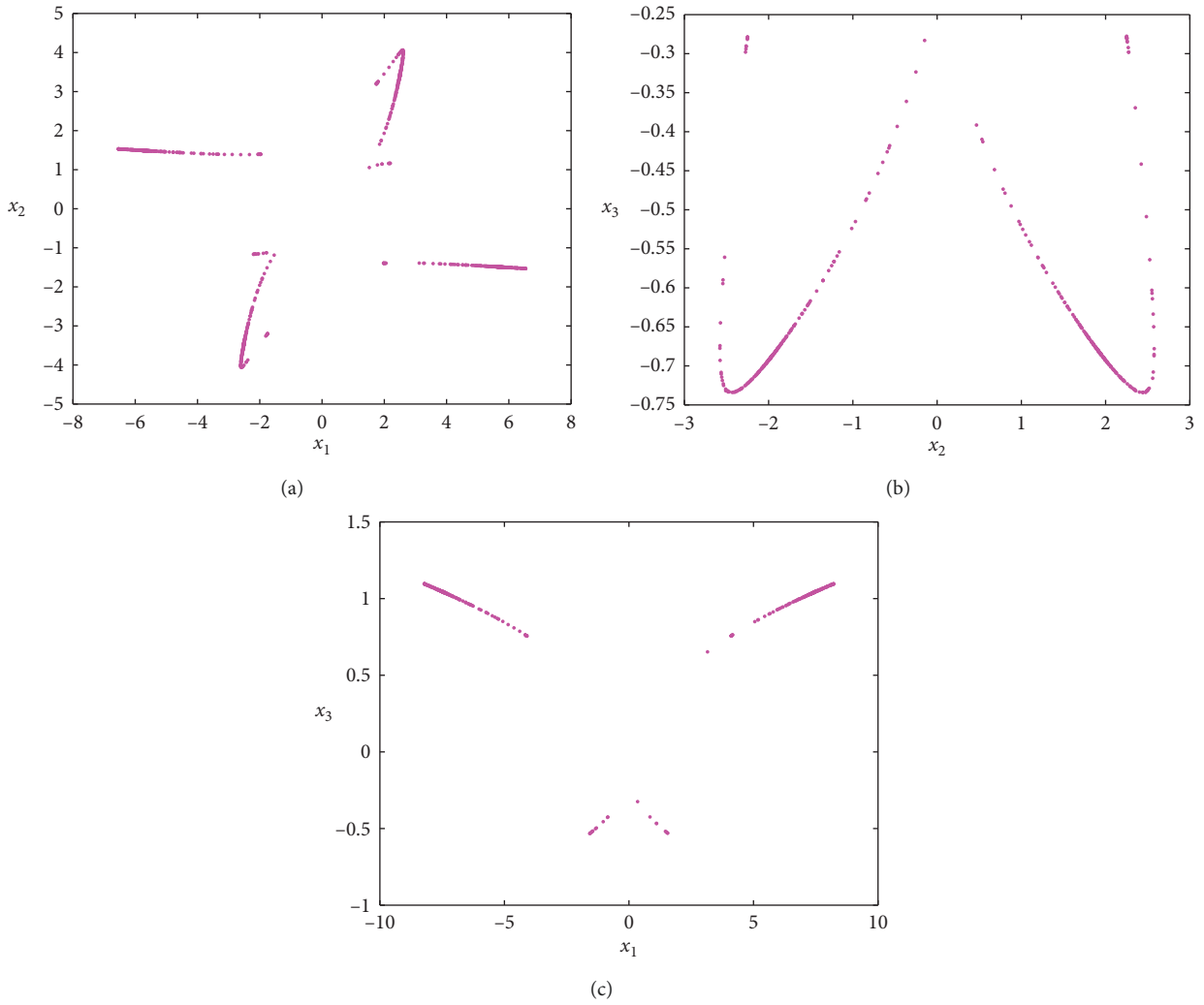

FIGURE 3: Poincaré maps on the plane of (a) $x_3 = 0$, (b) $x_1 = 0$, and (c) $x_2 = 0$.

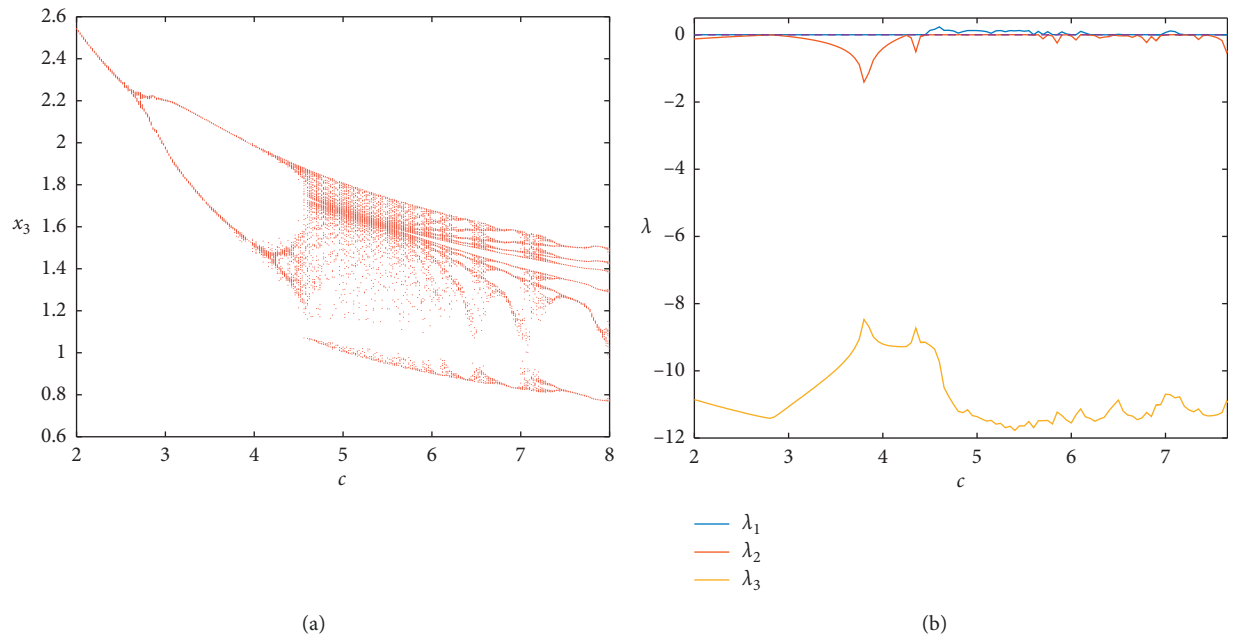

FIGURE 4: (a) Bifurcation diagram and (b) Lyapunov exponents of system (1) versus parameter c.

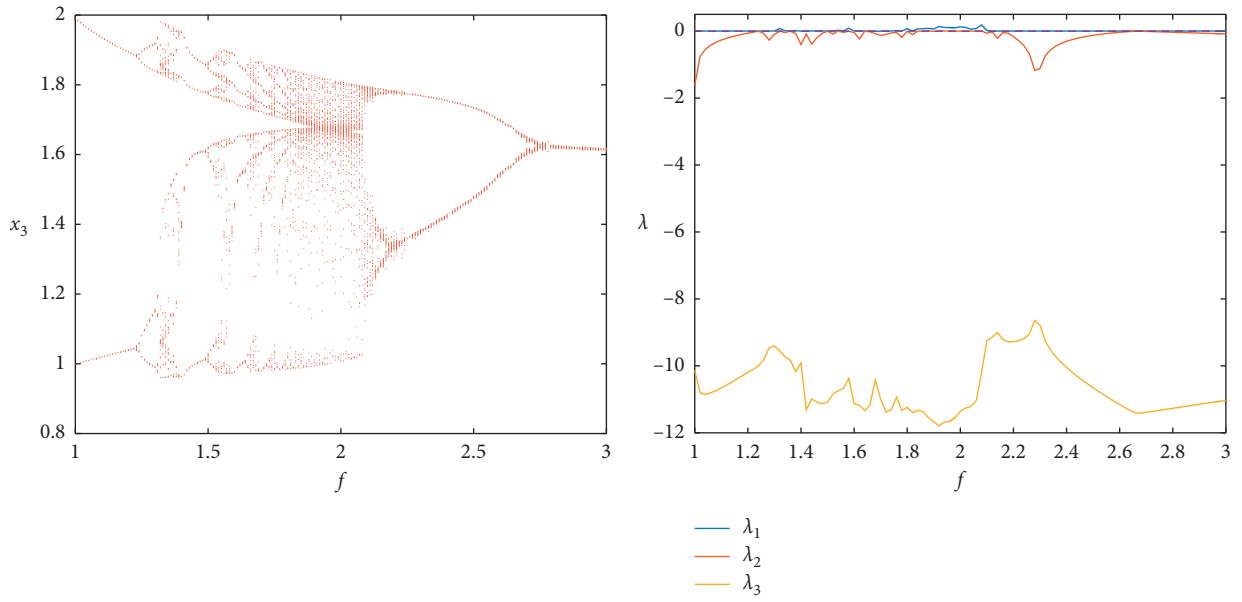

Figure 5: (a) Bifurcation diagram and (b) Lyapunov exponents of system (1) versus parameter f.

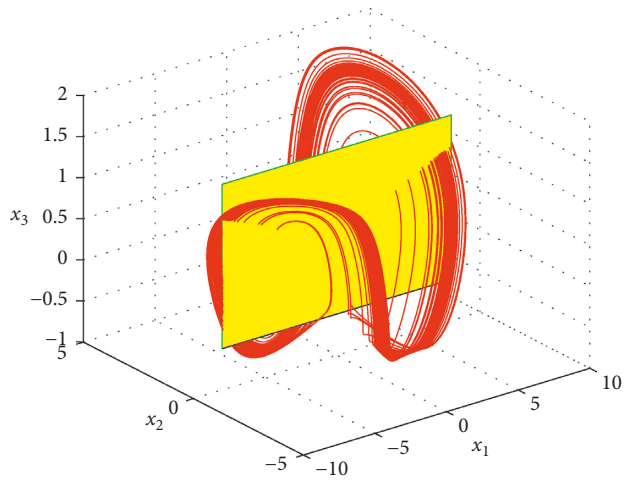

Figure 6: Poincaré cross section of the proposed system.

Step 3. Finally, we will take another quadrilateral D_2 of P such that $H(D_1) \longmapsto D_2$, $H(D_2) \longmapsto D_2$ and $H(D_2) \longmapsto D_1$. By a great deal of attempts, the four vertexes of D_2 are picked as follows:

$$\begin{aligned} &(-7.865357807, 0, 1.082029302)\\ &(-7.896026952, 0, 1.066318579)\\ &(-7.661826208, 0, 1.048363466)\\ &(-7.633945167, 0, 1.063232544). \end{aligned} \tag{5}$$

Analogously, D_2^1 and D_2^2 indicate the left and right sides of quadrilateral D_2, respectively. The numerical simulations of the third return Poincaré map $H^3(D_2)$ and the enlarged view are depicted in Figures 7(b) and 7(c), respectively. It is shown from the figures that the return map $H^3(x)$ $(x \in D_2)$ suitably across the quadrangles D_1 and D_2, with $H^3(D_2^1)$ lying on the right side of D_1 and $H^3(D_2^2)$ lying on the left side of D_2.

Therefore, we conclude by virtue of Lemma 2 that there would exist a compact invariant set $M \subset D$, such that $H^6 \mid M$ is semiconjugate to 2-shift dynamics, and we obtain $\text{ent}(H) \geq (\log 2)/6 > 0$. Thus, system (1) is proved to be chaotic in theory, with the parameters of $a = 1$, $b = 6$, $c = 5$, $d = 1$, $e = 3$, $f = 2$, and the initial condition of $x(0) = (0.01, 0.01, 0.05)$.

4. Stabilization for the Dynamical System

4.1. Control Scheme. In order to stabilize the proposed dynamical system, we add the single controller u on the second equation. Thus, the controlled dynamical system is depicted as follows:

$$\begin{cases} \dot{x}_1 = -ax_1 + bx_2, \\ \dot{x}_2 = ex_2 - fx_1x_3 + u, \\ \dot{x}_3 = -cx_3^3 + dx_1x_2. \end{cases} \tag{6}$$

The purpose of our design is to propose suitable control scheme u such that all the output variables of system (6) converge to the zero equilibrium point asymptotically.

Theorem 1. *For the controlled system (6), we design the single controller u as*

$$u = K\text{sign}(x_2). \tag{7}$$

If the control gain satisfies $K \leq -((b^2/4a) + e)B_2$ with $B_2 \geq \|x_2\|$, then the output variables of the controlled system (6) converges to the zero equilibrium point asymptotically.

Proof. We choose the candidate Lyapunov function as

$$V = 0.5\left(\frac{x_1^2 + x_2^2 + fx_3^2}{d}\right). \tag{8}$$

The corresponding time derivative of $V(x)$ is deduced by

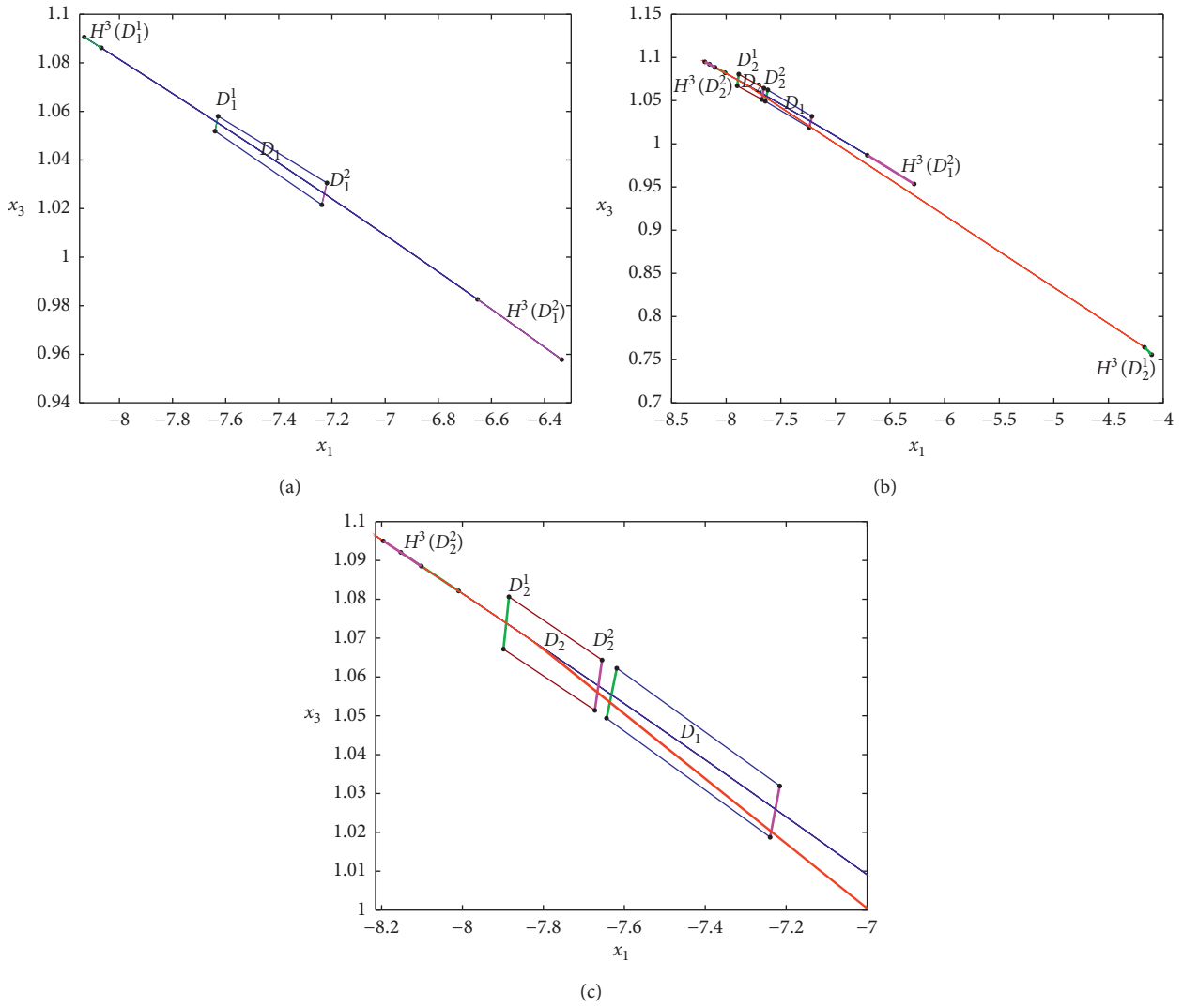

Figure 7: (a) The subset D_1 and its image; (b) and (c) the subset D_2 and its image.

$$\begin{aligned}
\dot{V} &= \frac{x_1\dot{x}_1 + x_2\dot{x}_2 + fx_3\dot{x}_3}{d} \\
&= -ax_1^2 + bx_1x_2 + ex_2^2 - fx_1x_2x_3 \\
&\quad + Kx_2\operatorname{sign}(x_2) - \frac{cfx_3^4}{d} + fx_1x_2x_3 \\
&= -ax_1^2 + bx_1x_2 + ex_2^2 + K|x_2| - \frac{cfx_3^4}{d} \\
&= -\left[ax_1^2 - bx_1x_2 + \left(\frac{b}{2\sqrt{a}}x_2\right)^2\right] + \left(\frac{b}{2\sqrt{a}}x_2\right)^2 \\
&\quad + ex_2^2 + K|x_2| - \frac{cfx_3^4}{d} \\
&= -\left[\sqrt{a}\,x_1 - \frac{b}{2\sqrt{a}}x_2\right]^2 + \left[\left(\frac{b^2}{4a} + e\right)|x_2| + K\right]|x_2| - \frac{cfx_3^4}{d}.
\end{aligned} \tag{9}$$

Thus, when $K \le -((b^2/4a) + e)B_2$, we find that

$$\begin{aligned}
\dot{V} &\le -\left[\sqrt{a}\,x_1 - \frac{b}{2\sqrt{a}}x_2\right]^2 + \left[\left(\frac{b^2}{4a} + e\right)B_2 + K\right]|x_2| - \frac{cfx_3^4}{d} \\
&\le -\left[\sqrt{a}\,x_1 - \frac{b}{2\sqrt{a}}x_2\right]^2 - \frac{cfx_3^4}{d} \le 0.
\end{aligned} \tag{10}$$

Therefore, the output variables of the controlled system (6) will converge to the zero equilibrium point asymptotically. □

4.2. Numerical Verification. In this section, numerical simulations are executed by adopting the ODE45 method to verify the availability of the proposed control scheme. For comparing conveniently, we choose the system parameters as $a = 1$, $b = 6$, $c = 5$, $d = 1$, $e = 3$, and $f = 2$, and the initial states are set as $x(0) = (0.01, 0.01, 0.01)$. With the parameter set, system (6) is chaotic before the controller is put into effect.

The controller u is exerted at 60th second, and the control gain is taken as $K = -2$ and $K = -16$. Figures 8(a) and 8(b) depict the control results, from which one can see that we can obtain good control effect with only taking a short time for the system to be stabilized at the fixed point. And, as we can also know only small control energy is needed to reach our control purpose.

5. DSP-Based Realization of the Attractors and Stabilization Scheme

The implementation of continuous chaotic systems with electronic circuit has been widely adopted. The parameter tolerance of the components of analog electronic circuit will cause the trajectory change of the chaotic system, which restricts its practical engineering application. Therefore, DSP-based implement of continuous chaotic system can overcome these problems effectively. In this section, the attractors of system (1) and stabilization scheme for system (6) are implemented based on the DSP platform. In our experiments, the Texas Instrument DSP TMS320F28335 is employed to calculate the state variable and the control variable, which can run at 150 MHz and interfaces with a 12-bit quad-channel digital-to-analog converter DAC7724 by parallel bus (PB) mode. Control signals required by DAC7724 are generated by DSP and CPLD chips. The block diagram of hardware platform is shown in Figure 9.

In practice, we discretize the continuous system by the classical fourth-order Runge–Kutta algorithm with the sampling period ΔT. From Figure 2, we know that the amplitude of variable x_3 ($|x_3| < 2$) is too small to affect the computational precision. Therefore, we proposed a general method to rescale the system variables by scaling factors k_i, where $i = 1, 2, 3$.

Setting $u_i = k_i x_i, i = 1, 2, 3$, system (1) can be transformed to

$$\dot{u}_i = f_i\left(a, b, c, d, e, f, k_1, k_2, k_3, u_1, u_2, u_3\right), \tag{11}$$

where $i = 1, 2, 3$.

When introducing the linear transformation of $u_i \longrightarrow x_i$, the corresponding differential equation of system (11) can be expressed as

$$\begin{cases} \dot{x}_1 = -ax_1 + \dfrac{bk_1}{k_2}x_2, \\ \dot{x}_2 = ex_2 - \dfrac{fk_2}{k_1k_3}x_1x_3, \\ \dot{x}_3 = -\dfrac{c}{k_3^2}x_3^3 + \dfrac{dk_3}{k_1k_2}x_1x_2. \end{cases} \tag{12}$$

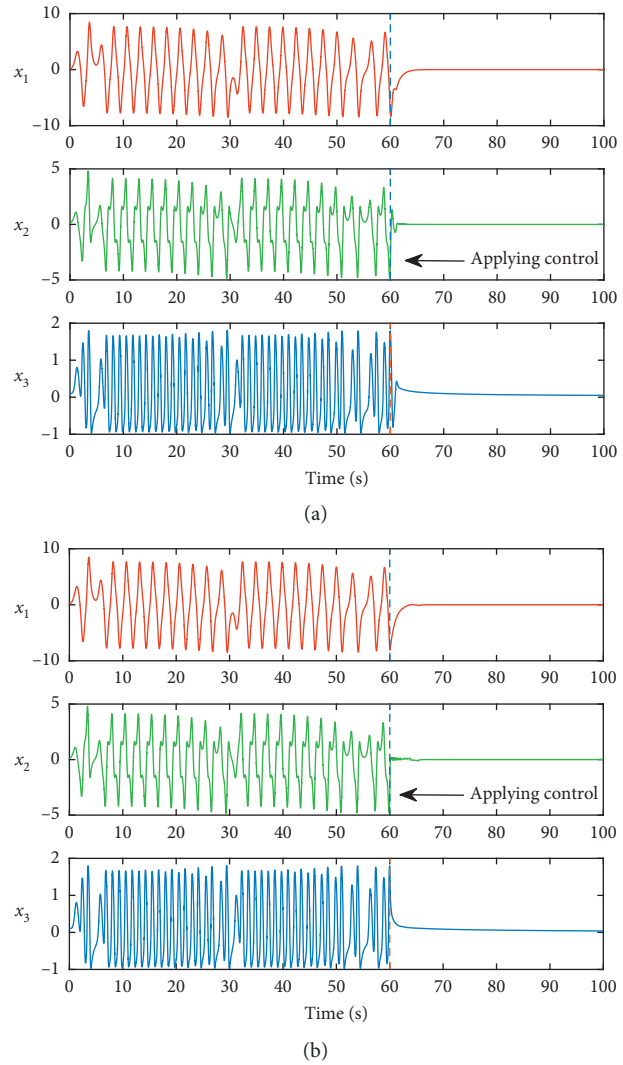

Figure 8: Control results of state variables with (a) $K = -2$ and (b) $K = -16$.

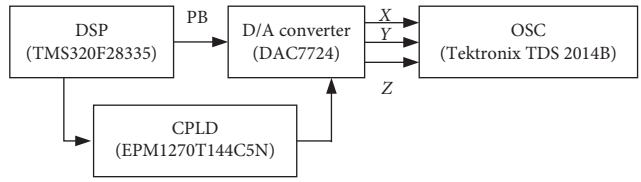

Figure 9: Block diagram for DSP implementation of chaotic attractors and its stabilization.

Discretizing system (12) using the classical fourth-order Runge–Kutta algorithm, the following difference equations can be obtained:

$$x_i(n+1) = x_i(n) + \Delta T \frac{\left(K_{i,1} + 2K_{i,2} + 2K_{i,3} + K_{i,4}\right)}{6}, \tag{13}$$

where $i = 1, 2, 3$ and

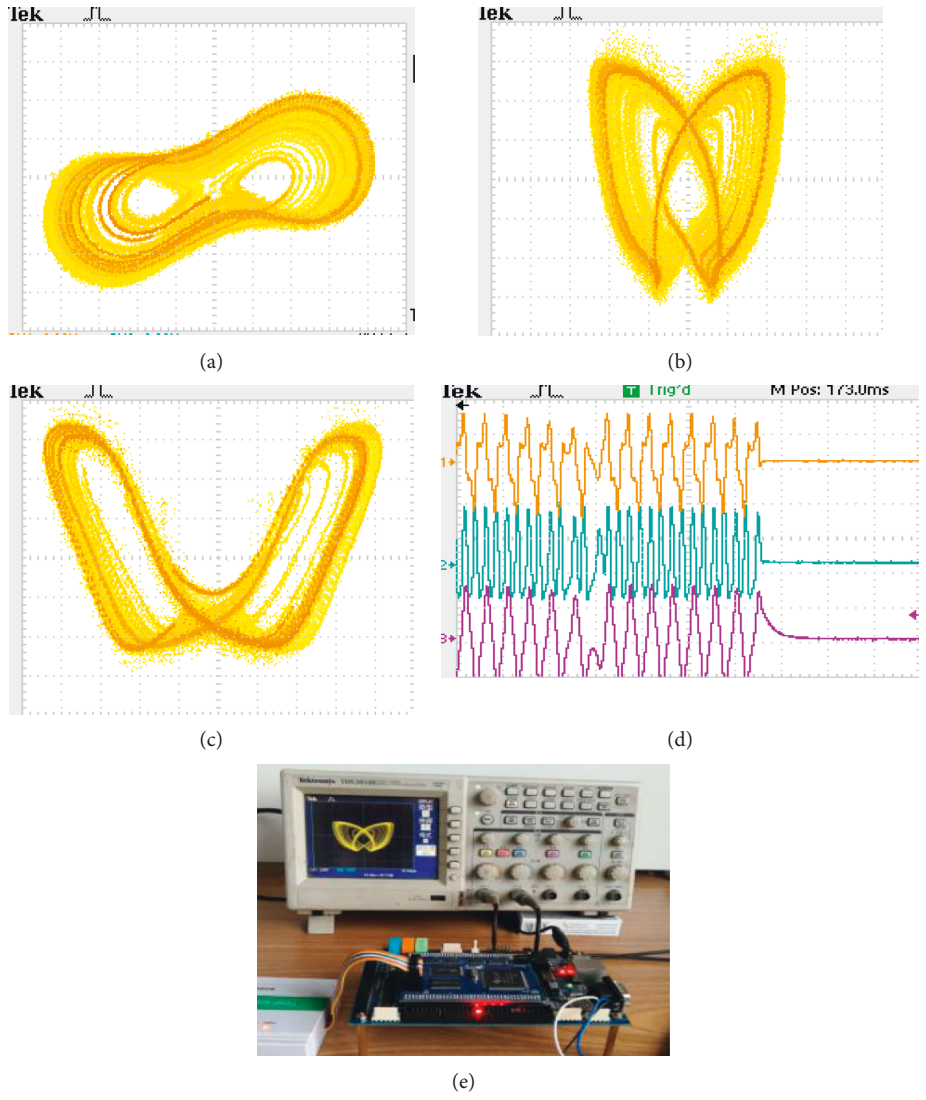

(a) (b) (c) (d) (e)

Figure 10: DSP-based realization for (a)–(c) chaotic attractors; (d) stabilization process; (e) experiment platform.

$$\begin{cases} K_{1,1} = -ax_1(n) + \dfrac{bk_1}{k_2}x_2(n), \\ K_{2,1} = ex_2(n) - \dfrac{fk_2}{k_1k_3}x_1(n)x_3(n), \\ K_{3,1} = -\dfrac{c}{k_3^2}x_3^3(n) + \dfrac{dk_3}{k_1k_2}x_1(n)x_2(n), \end{cases} \tag{14}$$

$$\begin{cases} K_{1,j} = -a\left[x_1(n) + mK_{1,j-1}\right] + \dfrac{bk_1}{k_2}\left[x_2(n) + mK_{2,j-1}\right], \\ K_{2,j} = e\left[x_2(n) + mK_{2,j-1}\right] - \dfrac{fk_2}{k_1k_3}\left[x_1(n) + mK_{1,j-1}\right]\left[x_3(n) + mK_{3,j-1}\right], \\ K_{3,j} = -\dfrac{c}{k_3^2}\left[x_3(n) + mK_{3,j-1}\right]^3 + \dfrac{dk_3}{k_1k_2}\left[x_1(n) + mK_{1,j-1}\right]\left[x_2(n) + mK_{2,j-1}\right]. \end{cases} \tag{15}$$

When $j = 2, 3$, $m = 0.5$, and when $j = 4$, $m = 1$.

The digital sequences $x_1(n), x_2(n), x_3(n)$ are produced by DSP according to (13)–(15) and converted into the corresponding analog sequences by the DAC7724 and then transmitted to oscilloscope. With the set $a = 1$, $b = 6$, $c = 5$, $d = 1$, $e = 3$, $f = 2$, $k_1 = 1$, $k_2 = 1$, $k_3 = 2$, $x(0) = (0.01, 0.01, 0.01)$, and the control gain $K = -6$, the results of DSP-based realization of the attractor and stabilization scheme are depicted in Figure 10. By comparing with the attractors in Figure 2 and stabilization process in Figure 7 simulated by Matlab, it can be concluded that they have a good qualitative agreement.

6. Conclusion

In this paper, we presented a three-dimensional dynamical system with a simple algebraic structure. Basic dynamical properties of the system, including equilibrium point, phase portrait, Poincaré map, parameter bifurcation, and Lyapunov exponent, are studied through theoretical analysis and numerical simulation. And, the theory of topological horseshoe is adopted to rigorously prove the chaotic emergence of the system theoretically. Then, based on the Lyapunov stability criterion, we designed a single control scheme to stabilize the chaotic system to its zero-equilibrium point. The attractor and stabilization process are realized via DSP-based technology, which have a good qualitative agreement to the Matlab simulation; thus it well confirmed the validity and enforceability of the theoretical scheme.

Data Availability

The figure data and table data used to support the findings of this study are included within the article.

Conflicts of Interest

The authors declare that there are no conflicts of interest regarding the publication of this paper.

Acknowledgments

This work was supported by the National Natural Science Foundation of China under Grant nos. 51977153 and 51577046, the State Key Program of National Natural Science Foundation of China under Grant no. 51637004, the National Key Research and Development Plan "Important Scientific Instruments and Equipment Development" under Grant no. 2016YFF0102200, the Equipment Research Project in Advance under Grant no. 41402040301, the Research Foundation of Education Bureau of Hunan Province of China under Grant no. 18A314, Hunan Provincial Natural Science Foundation of China under Grant no. 2019JJ40109, and the Science and Research Creative Team of Hunan Institute of Science and Technology (no. 2019-TD-10).

References

[1] J. Mou, K. Sun, J. Ruan, and S. He, "A nonlinear circuit with two memcapacitors," *Nonlinear Dynamics*, vol. 86, no. 3, pp. 1735–1744, 2016.

[2] J. Zhou, X. Wang, D. Xu, and S. Bishop, "Nonlinear dynamic characteristics of a quasi-zero stiffness vibration isolator with cam-roller-spring mechanisms," *Journal of Sound and Vibration*, vol. 346, pp. 53–69, 2015.

[3] F. Peng, Q. Long, Z.-X. Lin, and M. Long, "A reversible watermarking for authenticating 2D CAD engineering graphics based on iterative embedding and virtual coordinates," *Multimedia Tools and Applications*, vol. 78, no. 19, pp. 26885–26905, 2017.

[4] Z. Wei, Y. Li, B. Sang, Y. Liu, and W. Zhang, "Complex dynamical behaviors in a 3D simple chaotic flow with 3D stable or 3D unstable manifolds of a single equilibrium," *International Journal of Bifurcation and Chaos*, vol. 29, no. 7, p. 1950095, 2019.

[5] Y. Zhou, Z. Hua, C. M. Pun, and C. L. Chen, "Cascade chaotic system with applications," *IEEE Transactions on Cybernetics*, vol. 45, no. 45, pp. 2001–2012, 2015.

[6] M. Zapateiro, Y. Vidal, and L. Acho, "A secure communication scheme based on chaotic Duffing oscillators and frequency estimation for the transmission of binary-coded messages," *Communications in Nonlinear Science and Numerical Simulation*, vol. 19, no. 4, pp. 991–1003, 2014.

[7] C. Zhu, S. Xu, Y. Hu, and K. Sun, "Breaking a novel image encryption scheme based on Brownian motion and PWLCM chaotic system," *Nonlinear Dynamics*, vol. 79, no. 2, pp. 1511–1518, 2015.

[8] G. Ye, C. Pan, X. Huang, Z. Zhao, and J. He, "A chaotic image encryption algorithm based on information entropy," *International Journal of Bifurcation and Chaos*, vol. 28, no. 1, Article ID 1850010, 2018.

[9] X. Xiang and B. Shi, "Weak signal detection based on the information fusion and chaotic oscillator," *Chaos*, vol. 20, no. 1, Article ID 013104, 2010.

[10] Y. Ding, K. Sun, and X. Xu, "Hough-MHAF localization algorithm for dual-frequency continuous-wave through-wall radar," *IEEE Transactions on Aerospace and Electronic Systems*, vol. 52, no. 1, pp. 111–121, 2016.

[11] E. N. Lorenz, "Deterministic nonperiodic flow," *Journal of Atmospheric Sciences*, vol. 20, no. 2, pp. 130–141, 1963.

[12] J. Kennedy, S. Koçak, and J. A. YORKE, "A chaos lemma," *The American Mathematical Monthly*, vol. 108, no. 5, pp. 411–423, 2001.

[13] X.-S. Yang and Y. Tang, "Horseshoes in piecewise continuous maps," *Chaos, Solitons & Fractals*, vol. 19, no. 4, pp. 841–845, 2004.

[14] X.-S. Yang, "Topological horseshoes and computer assisted verification of chaotic dynamicsfication of chaotic dynamics," *International Journal of Bifurcation and Chaos*, vol. 19, no. 4, pp. 1127–1145, 2009.

[15] W.-Z. Huang and Y. Huang, "Chaos, bifurcation and robustness of a class of hopfield neural networks," *International Journal of Bifurcation and Chaos*, vol. 21, no. 3, pp. 885–895, 2011.

[16] C. Ma and X. Wang, "Hopf bifurcation and topological horseshoe of a novel finance chaotic system," *Communications in Nonlinear Science and Numerical Simulation*, vol. 17, no. 2, pp. 721–730, 2012.

[17] Q. Li and X.-S. Yang, "A simple method for finding topological horseshoes," *International Journal of Bifurcation and Chaos*, vol. 20, no. 2, pp. 467–478, 2010.

[18] C. Li, L. Wu, H. Li, and Y. Tong, "A novel chaotic system and its topological horseshoe," *Nonlinear Analysis: Modelling and Control*, vol. 18, no. 1, pp. 66–77, 2013.

[19] E. Ott, C. Grebogi, and J. A. Yorke, "Controlling chaos," *Physical Review Letters*, vol. 64, no. 11, pp. 1196–1199, 1990.
[20] K. Pyragas, "Continuous control of chaos by self-controlling feedback," *Physics Letters A*, vol. 170, no. 6, pp. 421–428, 1992.
[21] F. Farivar, M. A. Nekoui, M. A. Shoorehdeli, and M. Teshnehlab, "Modified projective synchronization of chaotic dissipative gyroscope systems via backstepping control," *Indian Journal of Physics*, vol. 86, no. 10, pp. 901–906, 2012.
[22] C. Li, K. Su, and L. Wu, "Adaptive sliding mode control for synchronization of a fractional-order chaotic system," *Journal of Computer Nonlinear Dynamics*, vol. 8, no. 3, Article ID 031005, 2013.
[23] E. Fridman, "A refined input delay approach to sampled-data control," *Automatica*, vol. 46, no. 2, pp. 421–427, 2010.
[24] A. B. MUZAFFAR and K. AYUB, "Multiswitching combination synchronization of non-identical fractional-order chaotic systems," *Pramana-J. Phys.*vol. 90, no. 6, 2018.
[25] Z. Wei, J. C. Sprott, and H. Chen, "Elementary quadratic chaotic flows with a single non-hyperbolic equilibrium," *Physics Letters A*, vol. 379, no. 37, pp. 2184–2187, 2015.
[26] A. T. Azar, C. Volos, N. A. Gerodimos et al., "A novel chaotic system without equilibrium: dynamics, synchronization, and circuit realization," *Complexity*, vol. 2017, no. 11, Article ID 7871467, 2017.
[27] G. Y. Peng, F. H. Min, and E. R. Wang, "Circuit implementation, synchronization of multistability, and image encryption of a four-wing memristive chaotic system," *Journal of Electrical and Computer Engineering*, vol. 2018, Article ID 8649294, 13 pages, 2018.